INL/RPT-25-84642

Diffusion Behavior of Oversized Fission Products in bcc Fe Cladding: A First-Principles Study

Technical Report

Jia-Hong Ke and Rongjie Song

Idaho National Laboratory

INL is a U.S. Department of Energy National Laboratory
operated by Batelle Energy Alliance, LLC

Diffusion Behavior of Oversized Fission Products in bcc Fe Cladding: A First-Principles Study

Technical Report

Jia-Hong Ke and Rongjie Song

Idaho National Laboratory

May 8, 2025

Idaho National Laboratory
Computational Mechanics and Materials Department
Irradiated Fuels and Materials Department
Idaho Falls, Idaho 83415

http://www.inl.gov

Prepared for the
U.S. Department of Energy
Office of Nuclear Energy
Under U.S. Department of Energy-Idaho Operations Office
Contract DE-AC07-05ID14517

Page intentionally left blank

Abstract

Fuel-Cladding Chemical Interaction (FCCI) poses significant challenges in nuclear reactors, where fission products from nuclear fuel interact with Fe-based cladding materials, potentially compromising their structural integrity. This study investigates the diffusion behavior of oversized fission products, Pr, Nd, Ce, and La, within bcc Fe cladding using density functional theory (DFT), nudged elastic band (NEB) method, and self-consistent mean field (SCMF) theory. Our results reveal significant vacancy binding energies, particularly with the 1st and 2nd nearest neighbors, which diminish beyond the 5th nearest neighbor, with La exhibiting the strongest binding affinity, followed by Nd, Ce, and Pr. The NEB calculations indicate significant high barriers for the dissociation of 1nn vacancy-solute pairs for all fission products. The tracer diffusion coefficients of these fission products was derived in Arrhenius form. The significant trapping effect of vacancies by a very dilute amount of fission products reduces vacancy mobility, leading to an oversaturation of point defects, void nucleation, and swelling. These are critical issues for irradiated cladding materials. The tracer diffusion coefficients indicate that Nd diffuses the fastest, followed by La, Ce, and Pr. This study provides essential insights for developing advanced cladding materials and design strategies to mitigate FCCI, ultimately enhancing nuclear reactor safety and performance.

Page intentionally left blank

Acknowledgments

This report was authored by a contractor of the U.S. Government under contract DE-AC07-05ID14517. Accordingly, the U.S. Government retains a non-exclusive, royalty-free license to publish or reproduce the published form of this report, or allow others to do so, for U.S. Government purposes. This research made use of the resources of the High Performance Computing Center at Idaho National Laboratory, which is supported by the DOE Office of Nuclear Energy and the Nuclear Science User Facilities under contract no. DE-AC07-05ID14517.

Page intentionally left blank

Contents

List of Figures

List of Tables

1. Introduction

Fuel-Cladding Chemical Interaction (FCCI) is a critical phenomenon that occurs in nuclear reactors, where fission products from the nuclear fuel interact with the cladding materials, such as Fe-based alloys [1, 2, 3, 4]. Due to the infiltration of fission products into the cladding materials, FCCI can potentially compromising its structural integrity. The cladding serves as the first line of protection, preventing the release of radioactive fission products into the coolant and environment. Therefore, understanding the transport behavior of fission products within the cladding is essential for ensuring the long-term safety and performance of nuclear reactors.

In particular, the study of fission product transport within the body-centered cubic (bcc) Fe cladding is of significant interest [3]. Fission products or lanthanides such as praseodymium (Pr), neodymium (Nd), cerium (Ce), and lanthanum (La) are known to be oversized atoms. Their diffusion behavior in the cladding material can lead to the formation of brittle phases on grain boundaries, swelling, and other deleterious effects that degrade the mechanical properties [4, 5]. The limited diffusion data for these fission products in bcc Fe poses a challenge to our comprehensive understanding of FCCI and the associated rate processes.

To address this challenge, advanced computational methods are employed to predict the transport behavior of these fission products. In this work, we utilize density functional theory (DFT), nudged elastic band (NEB) method to calculate the migration barrier of vacancy-mediated diffusion of Pr, Nd, Ce, and La in bcc Fe. DFT provides a quantum mechanical description of the electronic structure, enabling accurate predictions of atomic interactions and diffusion pathways. The migration barriers can be used by the multi-frequency diffusion models to calculation transport coefficients, such as tracer diffusion coefficients, vacancy diffusivity, and Onsager transport coefficients that describe the kinetic coupling between solute atoms and defects [6]. However, the traditional multi-frequency models, which are often used to describe diffusion in crystalline solids, may not be sufficient for these oversized atoms due to their unique diffusion mechanisms compared to typical diffusion of solute atoms that can be mapped onto the perfect bcc lattice [7].

Notably, the interaction between fission products and vacancies in the cladding material extends over long ranges, which complicates the diffusion process. The binding energy between fission products and vacancies, as well as their interaction energies, must be accurately accounted for to predict diffusion behavior. The self-consistent mean field (SCMF) theory, which considers long-range interactions and collective effects of diffusion, is therefore necessary to capture the complexity of these diffusional processes and predict the fission product transport coefficients [8, 9].

Understanding the diffusion behavior of fission products such as Pr, Nd, Ce, and La in bcc Fe is critical for predicting the long-term performance and safety of nuclear fuel cladding. The insights gained from these simulations can inform the development of improved cladding materials and design strategies to mitigate the adverse effects of FCCI. This

study aims to provide quantitative prediction and understanding of fission product transport in bcc Fe cladding through the use of DFT and SCMF. The results will offer valuable insights into the diffusion mechanisms of oversized fission products and their interactions with the cladding material, ultimately contributing to the development of new cladduing materials.

2. Methods

To investigate the diffusion behavior of fission products (Pr, Nd, Ce, and La) in bcc Fe cladding, we employ a combination of DFT, NEB and SCMF methods. This methodological approach allows us to accurately predict tracer diffusion coefficients by accounting for long-range interactions and the complex diffusion mechanisms of oversized atoms. In the following, the detail of the diffusion model based on the SCMF will be described, followed by the method to calculate the binding energies and migration barriers required to derive transport coefficients by SCMF.

2.1 Diffusion model and self-consistent mean field (SCMF) approach

Le Claire's multi-frequency model has been widely used to describe atomic diffusion in metals, accounting for different jump frequencies of atoms between various lattice sites [6, 10]. However, this model may be inadequate for oversized atoms, such as the fission products Pr, Nd, Ce, and La, in bcc Fe. Oversized atoms have significantly larger atomic radii compared to the host lattice atoms, leading to substantial lattice distortions and unique diffusion pathways that are not adequately captured by the multi-frequency model, which typically assumes atomic jumps following the lattice structure. Additionally, the interactions between oversized atoms and vacancies, as well as among different oversized atoms, tend to be long-range and complex. The multi-frequency model generally considers short-range interactions and assumes a relatively simple energy landscape, which is insufficient for accurately describing the behavior of oversized atoms.

To overcome these limitations, we employ the SCMF method, which is capable of capturing the intricate dynamics of oversized atoms and their interactions with vacancies. The SCMF method is a powerful theoretical framework used to study atomic transport in solids[9]. This approach is particularly effective in addressing the complexities of diffusion mechanisms involving point defects and solute atoms in various crystalline materials. The SCMF theory simplifies the diffusion problem by representing kinetic correlations through a non-equilibrium effective Hamiltonian and the use of cluster transport coefficients. The latter is defined as a linear combination of transport coefficient of non-overlapping clusters with their concentrations. The kinetic coefficients are therefore expanded in terms of cluster contributions, in a form similar as the kinetic version of cluster expansion [8]. The SCMF approach has been applied to study diffusion of minor alloying elements in steels in attempts to investigate irradiated microstructure tendency such as radiation-induced segregation [11, 12, 13, 14].

In this research, we employ the SCMF tool, KineCluE [8], to investigate the transport of fission products, specifically Pr, Nd, Ce, La, in bcc Fe. By systematically increasing the range of kinetic interactions, we can derive kinetic

coefficients that converge to the exact solution for a single cluster in an infinite medium. This approach enables us to capture the essential features of fission product transport, such as the impact of kinetic correlations on the diffusion process.

We follow the previous diffusion study to consider a network of the 12 Fe-Va jump frequencies affected by the presence of a solute atom, for solute-vacancy interactions extending to the 5nn distance [11], with maximum distance of the vacant site at 10nn. The network of the diffusion model is shown in Figure 1. The solute-vacancy exchange is labeled with ω_2 , and ω_0 represents the unaffected Fe-Va jump frequency. For the rest of the diffusion jump labels ω_{ij}, they represents the jump from the start position i to the end position j, where i represent the i-th nearest neighbor (nn) atoms around the fission product atom. By following the framework of transition state theory, the jump frequency ω_{ij} for the vacancy moving from site i to site j is $\omega_{ij} = \upsilon_{ij}\exp(-E^{ij}_{\text{mig}}/kT)$, where υ_{ij} is the attempt frequency, E^{ij}_{mig} is the migration barrier, k is the Boltzmann constant, and T is the temperature. Since υ_{ij} is typically at the magnitude of 10 THz and the exact value does not strongly influence the activation energy of vacancy-mediated diffusion, the attempt frequency is assumed to be the same for considered jumps and of the same order of magnitude of the Debye frequency in Fe, which is 6 THz [11].

Note that during the structural optimization by DFT for the 1nn vacancy pair with the oversized fission product, the atom are found to relax to the ground-state position at the center between the original solute atom and the 1nn site. In other words, the two diffusion ground states of the ω_2 jump are indistinguishable. As a consequence, the ω_2 jump is prohibited as the oversized atom splits the vacant site in half. The diffusion of oversized atoms cannot be described by the typical vacancy mechanism such as that assumed in the multi-frequency model. To account for the diffusion of oversized solute atom, the mechanism proposed by Bocquet et al. [7] was applied in the SCMF simulations.

The solute-vacancy binding energies and the migration barriers of atom jumps as illustrated in Figure 1 are required for the KineCluE code to calculate the transport coefficients. These important energies can be derived by first-principles

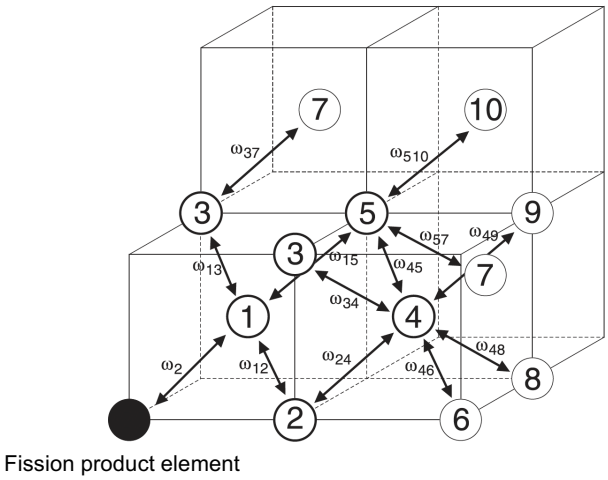

Figure 1. Schematic showing the network of the 12 Fe-Va jump frequencies affected by the presence of a solute atom for us in the SCMF modeling of fission product diffusion. The figure is adapted from [11].

DFT calculations. The computational methods and settings of DFT calculations are detailed in the next section.

2.2 First-principles methods

The vacancy-solute interactions and the migration barriers described in Section 2.1)are calculated using the Vienna Ab initio Simulation Package (VASP)[15, 16], a quantum mechanical density functional theory-based code. All calculations were spin-polarized and initialized under the ferromagnetic ordering. We adopted the previous approach of ab initio calculations predicting diffusion properties of dilute Ni-based alloys [17, 18, 19]. The plane wave energy cutoff was selected to be 400 eV for all calculations. The interactions between ions and core electrons are described using the projector augmented wave (PAW) method [20, 21] and the Perdew-Burke-Ernzerhof parameterization [22] of the generalized gradient approximation (GGA) was used for the exchange correlation potentials. The k-point mesh was generated automatically using the Monkhorst-Pack scheme. Calculations were performed with a 128 atom periodic simulation cell. The simulation cell is a $4\times4\times4$ supercell of the bcc conventional cell with a lattice parameter of 2.83 Å. The k-point mesh describes the sampling of the Bravais lattice and a $4\times4\times4$ mesh was used for all calculations.

The vacancy-solute binding energies from 1nn to 10nn are calculated by the following equation [17],

$$E^{\mathrm{X}}_{\mathrm{vb,\ i\text{-}nn}} = E(126\mathrm{Fe} + 1\mathrm{X} + 1\mathrm{Va}_{\mathrm{i\text{-}nn}})_{\Omega} - E(127\mathrm{Fe} + 1\mathrm{Va}_{\mathrm{i\text{-}nn}})_{\Omega} - E(127\mathrm{Fe} + 1\mathrm{X})_{\Omega'} + E(128\mathrm{Fe})_{\Omega'}, \qquad (2.1)$$

where E is the energy calculated by DFT, X denotes the solute or fission product atom at the origin, and Va denotes the vacancy at the different nearest neighbor distance (i-nn) from the fission product atom X (as described in Figure 1). The energy of the isolated vacancy and fission product atom are subtracted separately from the energy of the system where they interact, and then the energy of a perfect, un-defected bcc Fe is added for mass balance. We adopt the sign convention that the negative binding energy indicates the energetically favorable binding of a solute with a vacancy. Calculations were performed with the bcc supercell where the volume and shape are fixed but ionic relaxations are allowed. Note that the volumes of the solute-containing simulations cells are identical with the volumes of the pure Fe cells, regardless of the presence of the vacancy (Ω and Ω' for the volume with and without a vacancy, respectively).

Migration barriers for vacancy hopping between the two ground-state lattice sites were calculated by using the CI-NEB (Climbing Image-Nudged Elastic Band) method [23, 24] with three intermediate migration images for all atomic hops. A cubic spline was fitted to the migration energy landscape and the barrier was determined by taking the energy difference between the saddle point with respect to the energy at the two end configurations. The saddle point represents the configuration where the energy is maximum in the migration energy profile. The Quick-Min force-based optimizer was used to determine the minimum energy paths and saddle points, and the optimizer was implemented by the Transition State Tools for VASP (VTST). In all CI-NEB runs, the break condition of energy convergence for electronic relaxation is 10^{-5} eV and that of force for ionic relaxation is 0.01 eV/Å.

2.3 Magnetic correction

To account for the transition from the ferromagnetic to paramagnetic state in bcc Fe at finite temperatures, the magnetic correction model used by [11] was adopted. This correction utilizes the Hillert-Jarl phenomenological model [25]. The activation energy of the vacancy-mediated diffusion decreases proportionally to the magnetic excess enthalpy by:

$$Q = Q_0^F - (Q_0^F - Q^P)H(T) \tag{2.2}$$

where Q is the activation energy of diffusion, Q_0^F and Q^P are the activation energies at the ferromagnetic and paramagnetic states, which are 2.86 and 2.26 eV, respectively, and H(T) is a temperature-dependent factor related to the ratio of magnetic enthalpy at finite temperature and that at zero K by $H(T) = 1 - H^{\mathrm{mag}}(T)/H^{\mathrm{mag}}(0)$.

Following Hillert-Jarl model [25], $H^{\mathrm{mag}}(T)$ can be expressed by

$$H^{\mathrm{mag}}(T) = RT_C \ln(B+1) f(\tau) \tag{2.3}$$

where R is the gas constant, T_C is the Curie temperature of Fe (1043 K), B is the magnetic moment of Fe (2.22 Bohr magnetons) and $\tau = T/T_C$. The function $f(\tau)$ can be expressed as

$$f(\tau) = \frac{1}{A}\frac{79}{140P} - \frac{474}{497}\left(\frac{1-P}{P}\right)\left(\frac{\tau^4}{2} + \frac{\tau^{10}}{15} + \frac{\tau^{16}}{40}\right) (\tau < 1) \tag{2.4}$$

$$f(\tau) = \frac{1}{A}\left(\frac{\tau^{-4}}{2} + \frac{\tau^{-14}}{21} + \frac{\tau^{-24}}{60}\right) (\tau \geq 1) \tag{2.5}$$

where

$$A = \frac{518}{1125} + \frac{11692}{15975}\left(\frac{1-P}{P}\right) \tag{2.6}$$

and P is a geometry factor (0.40) for bcc crystals.

Note that Eq. 2.2 was originally developed for self-diffusion in bcc Fe, but it can also be extended to solute diffusion and vacancy mobility by assuming that a dilute amount of solutes (e.g., fission products) produces negligible effects on the correlation between magnetic configuration and vacancy-mediated diffusion properties. The temperature-dependent magnetic correction can be expressed by the factor $\exp\left[\left(Q_0^F - Q^P\right) H(T)/kT\right]$. The temperature dependent correction factor is shown in Figure 2. The correction factor is close to one (no correction) at low temperature as the ferromagnetic configuration dominates, and the factor has sharp increase to $\sim$ 102 as the temperature increases beyond T_C (1043 K).

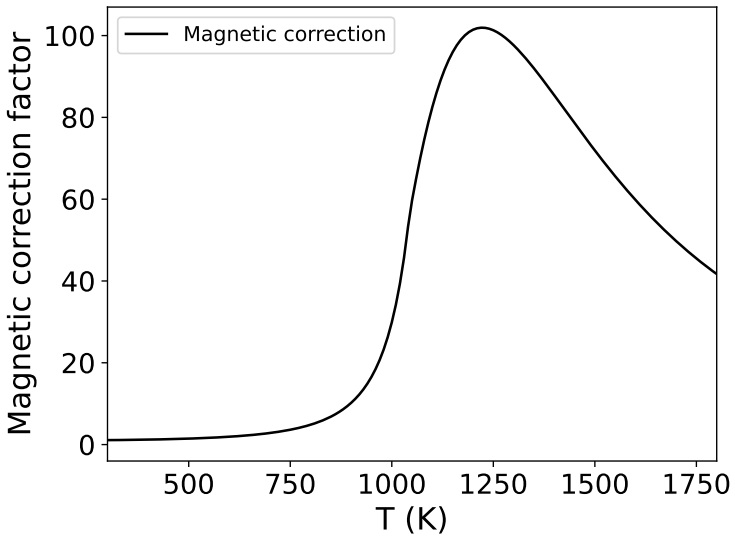

Figure 2. Plots showing the magnetic correction factor exp $\left[\left(Q_0^F - Q^P\right) H(T)/kT\right]$ accounting for the transition from the ferromagnetic to paramagnetic state in bcc Fe at finite temperatures.

3. Results and discussion

3.1 Vacancy binding

Figure 3 and Table 3.1 show the DFT calculation results of the binding energy of vacancy-fission-product pairs from the 1nn to the 10nn. The results reveal significant long-range vacancy binding in bcc iron, which diminishes beyond the 6nn for all the fission products. This indicates strong long-range interactions of oversized fission product elements with vacancies within the bcc-Fe matrix. It also highlights the inadequacy of Le Claire's multi-frequency approximation, which considers interactions up to the second nearest neighbor. Therefore, SCMF theory is needed for more comprehensive modeling approaches to accurately capture the transport behavior of fission products in bcc Fe.

Table 3.1. DFT calculation results of binding energies of fission products (La, Pr, Ce, and Nd) and vacancies from 1nn to 10nn. The unit of binding energy is in eV.

Fission product	1nn	2nn	3nn	4nn	5nn	6nn	7nn	8nn	9nn	10nn
Nd	-1.64	-0.35	-0.08	-0.01	-0.14	0.01	0.03	0.02	0.04	0.03
Ce	-1.56	-0.33	-0.05	-0.02	-0.09	0.04	0.04	0.02	0.03	0.02
Pr	-1.39	-0.40	-0.03	-0.05	-0.03	0.04	0.02	0.02	0.02	-0.01
La	-1.72	-0.47	-0.05	-0.01	-0.11	0.05	0.03	0.02	0.03	0.03

The binding energies indicate the order of 1nn vacancy binding as La > Nd > Ce > Pr. This observed trend provides insights into the varying degrees of interaction between different fission products and vacancies. Notably, all the 1nn binding energies are at the magnitude of $\sim$ 1.4 eV or higher, suggesting a significant attractive interaction that cause vacancy trapping. The observation that the 5nn exhibits slightly stronger vacancy binding than 3nn and 4nn, possibly due to the close-packed <111> directional long-range vacancy-solute pair interaction that accommodate the vacant site, highlights the complexity and anisotropy of these interactions. This directional dependence suggests that certain crystallographic directions may facilitate stronger binding, potentially influencing the overall diffusion pathways of vacancies and solutes.

The significant trapping effect of vacancies by infiltrated fission products in Fe-based cladding has important implications for material behavior under irradiation. While the trapping of vacancies can typically increase the importance of point defect recombination, the low density of these traps (due to extremely low solubility of fission products in the matrix) may limit their beneficial effects. Instead, the trapping effect is more likely to slow down the kinetics of

vacancy migration, as additional energy is required for vacancies to dissociate from the bound pairs. Additionally, the attractive binding interaction beyond the 1nn may also contribute to a larger capture radius of traps compared to non-oversized solute atoms.

Reduced vacancy mobility makes vacancies less likely to migrate to sinks, such as grain boundaries or dislocations, where they can be annihilated. This potentially leads to a higher concentration of excess vacancies within the cladding material in irradiated environments, promoting the nucleation and growth of voids, and contributing to void swelling, which is a critical issue for cladding materials subjected to irradiation. In the next section, the effect of dilute fission products on vacancy mobility will be presented.

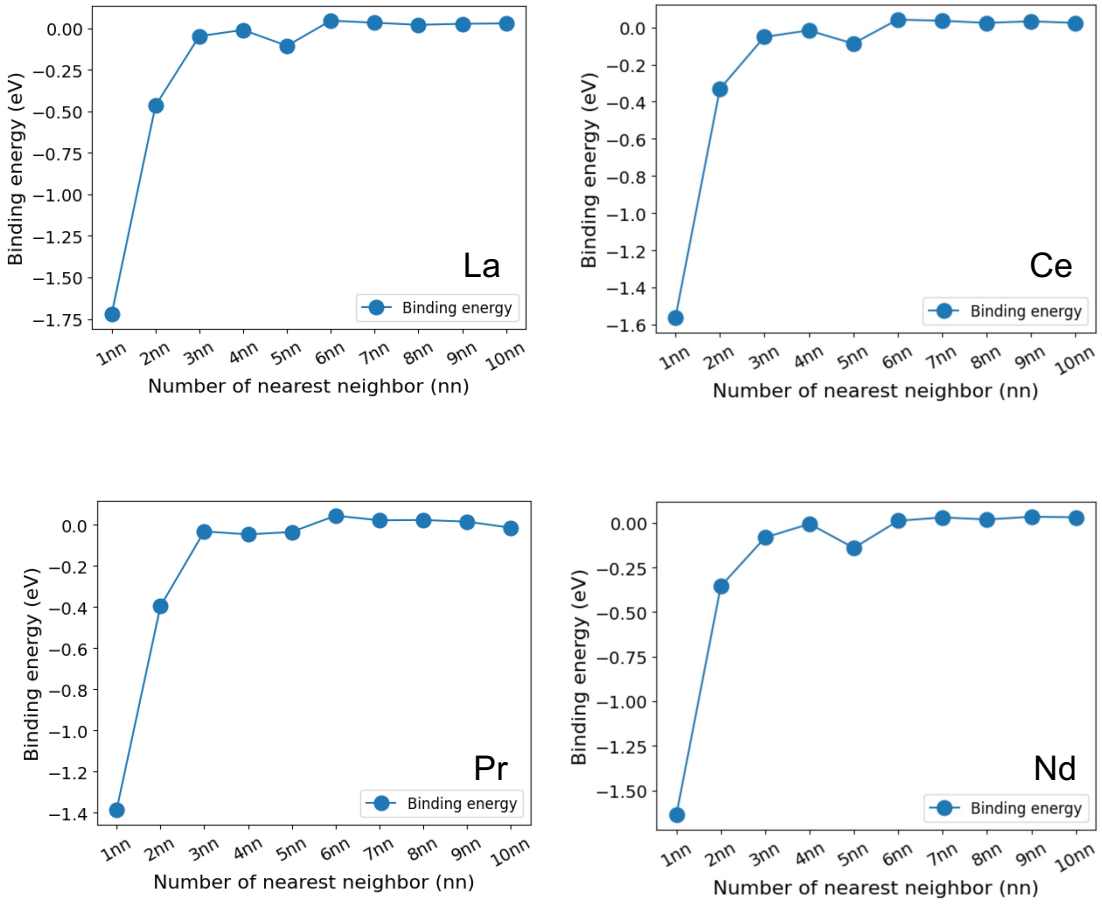

Figure 3. Plots showing the calculated binding energies of fission products (La, Pr, Ce, and Nd) and vacancies from 1nn to 10nn.

3.2 Migration barrier

The migration barriers associated with the 12-frequency framework (Figure 1) are summarized in Table 3.2. For pure Fe without fission products, the migration barrier of Fe is calculated as 0.68 eV, consistent with latest literature [11]. For all fission products, the migration barriers involving the dissociation of 1nn vacancy-solute pairs (ω_{12}, ω_{13}, and ω_{15}) are significant higher than those of the other atomic jump, in a order following La > Nd ≈ Ce > Pr. The significantly higher migration barriers of 1nn vacancy dissociation (ω_{12}, ω_{13}, and ω_{15}) than association hops (ω_{21}, ω_{31}, and ω_{51}) indicates strong 1nn vacancy binding. This observed result is consistent with the binding energies presented in Section 3.1.

Note that for all these fission products, the migration barriers of the association hop ω_{51} is very low, especially for La and Nd. This observation indicates that while the state of 5nn is considered a local ground state at 0K based on the structural optimization during DFT calculations, the stability of this configuration is very low as it can be relaxed to 1nn by small lattice perturbations that can easily overcome the energy barrier of approximately 0.01 eV for Nd and La.

As the atomic hops are beyond the 5nn around the fission product atom, the migration barriers become similar to that of ω_0, as shown in Table 3.2. This observation suggests that the effect of fission product atom on migration barrier diminishes beyond 5nn, which is similar to the influence of fission product on the vacancy binding energy. The only exceptions are the atomic hops that are associated with the vacancy at the close-packed <111> direction (e.g., 5nn and 10nn) with respect to the position of fission product atom. For example, the migration barriers of ω_{54}, ω_{75}, ω_{105} are evidently different from that of ω_0 even when their hopping events are not close to the fission product atom.

Table 3.2. DFT calculation results of all migration barriers (eV) of hops described in Section 2.1.

Hopping path	La	Ce	Pr	Nd
ω_0 (pure Fe)	0.68	0.68	0.68	0.68
ω_{12}, ω_{21}	2.48, 1.12	2.25, 1.02	2.00, 1.01	2.31, 1.03
ω_{13}, ω_{31}	1.92, 0.13	1.72, 0.21	1.66, 0.31	1.70, 0.15
ω_{15}, ω_{51}	1.62, 0.01	1.50, 0.03	1.45, 0.10	1.50, 0.01
ω_{24}, ω_{42}	0.88, 0.37	0.78, 0.47	0.83, 0.48	0.79, 0.44
ω_{34}, ω_{43}	0.77, 0.69	0.74, 0.71	0.69, 0.71	0.77, 0.70
ω_{37}, ω_{73}	0.63, 0.52	0.66, 0.58	0.66, 0.60	0.65, 0.53
ω_{45}, ω_{54}	0.69, 0.78	0.69, 0.76	0.65, 0.64	0.69, 0.78
ω_{46}, ω_{64}	0.71, 0.68	0.73, 0.67	0.71, 0.69	0.71, 0.69
ω_{48}, ω_{84}	0.66, 0.64	0.68, 0.64	0.67, 0.64	0.67, 0.65
ω_{49}, ω_{94}	0.66, 0.62	0.67, 0.62	0.66, 0.60	0.64, 0.60
ω_{57}, ω_{75}	0.72, 0.58	0.71, 0.59	0.67, 0.61	0.73, 0.56
ω_{510}, ω_{105}	0.67, 0.54	0.68, 0.57	0.65, 0.63	0.69, 0.51

3.3 Kinetic coefficients determined by SCMF

The calculated binding energies and migration barriers presented in Sections 3.1 and 3.2 are incorporated into the KineCluE code to calculate transport coefficients, including the tracer diffusion coefficients of Pr, Nd, Ce, and La, as well as the influence of these fission products on vacancy diffusivity. The tracer diffusion coefficients provide valuable insights into the rate processes of fission product infiltration into the matrix of cladding materials, while the information on vacancy diffusivity highlights the efficiency of vacancy annihilation by diffusion to sinks.

To correctly model the diffusion mechanism of oversized atoms, it is important to forbid the 1nn configuration before structural relaxation, as the oversized atom occupies the center of the relaxed 1nn pair after structural optimization. This can be achieved in the KineCluE interaction file by setting the prefactor of the binding energy associated with the unrelaxed 1nn vacancy-solute pair to zero and adding the relaxed configuration with X at $(0.25a, 0.25a, 0.25a)$ and Va at $(0.25a, 0.25a, 0.25a)$, where X is the fission product atom and a is the lattice spacing of the bcc Fe. Additionally, in the interaction file for running the KineCluE code, it is required to define the saddle point energies (E_{sp}) with respect to the binding energies by $E_{sp}^{i\to j} = E_{mig}^{i\to j} - E_{vb,i\text{-}nn}$, where E_{mig} is the migration barrier calculated by the CI-NEB method.

Figure 4 (a) shows the SCMF calculation results of the tracer diffusion coefficients of Pr, Nd, Ce, and La in bcc Fe with the magnetic correction, and Figure 4 (b) shows the same diffusion coefficients in ferromagnetic bcc Fe without the correction. The calculated self-diffusion coefficient of Fe is also included in Figure 4 for comparison. The calculated self-diffusion coefficient of Fe shows excellent agreement with [11]. The results indicate that Nd is the fastest diffuser among the four fission products, followed by La, Ce, and Pr. Nevertheless, it can be seen in Figure 5 that the diffusion behaviors of all these four fission products are similar due to their oversized nature and the similarities of their binding interactions with vacancies and migration barriers, as detailed in Section 3.1 and 3.2. The tracer diffusion coefficients of Nd, La, Ce, and Pr in ferromagnetic bcc Fe, as well as the self-diffusion coefficient of ferromagnetic Fe, can be fitted against the Arrhenius equation:

$$D_{\mathrm{Nd}}^{*\mathrm{ferro}} = 4.89\times10^{-5}\exp\left(-\frac{2.25(\mathrm{eV})}{kT}\right)(\mathrm{m}^2/\mathrm{s}), \tag{3.1}$$

$$D_{\mathrm{La}}^{*\mathrm{ferro}} = 5.23\times10^{-5}\exp\left(-\frac{2.31(\mathrm{eV})}{kT}\right)(\mathrm{m}^2/\mathrm{s}), \tag{3.2}$$

$$D_{\mathrm{Ce}}^{*\mathrm{ferro}} = 5.28\times10^{-5}\exp\left(-\frac{2.34(\mathrm{eV})}{kT}\right)(\mathrm{m}^2/\mathrm{s}), \tag{3.3}$$

$$D_{\mathrm{Pr}}^{*\mathrm{ferro}} = 7.06\times10^{-5}\exp\left(-\frac{2.47(\mathrm{eV})}{kT}\right)(\mathrm{m}^2/\mathrm{s}), \tag{3.4}$$

$$D_{\mathrm{Fe}}^{\mathrm{ferro}} = 8.62\times10^{-5}\exp\left(-\frac{2.86(\mathrm{eV})}{kT}\right)(\mathrm{m}^2/\mathrm{s}). \tag{3.5}$$

Note that the difference between Figure 4 (a) and (b) is negligible at temperatures lower than $\sim$ 750 K due to the dominance of ferromagnetic state, and therefore the diffusion coefficients can well be described by Eq. 3.1 - Eq. 3.5. However, to account for the magnetic transition at high temperatures, the correction factor $\exp\left[\left(Q_0^F - Q^P\right)H(T)/kT\right]$

should be included in these equations to generate the results shown in Figure 4 (a).

Figure 5 (a)-(d) illustrates the impact of dilute fission products on vacancy diffusivity at 600 - 1200 K. The strong binding affinity between fission product atoms and vacancies is anticipated to immobilize mobile vacancies, thereby reducing their mobility. The effect of reduced mobility is particularly strong at lower temperatures, even when the concentration of fission products is extremely dilute, as seen at 600 K in Figure 5 (a). Among the fission products investigated, La exhibits the strongest trapping effect, followed by Nd, Ce, and Pr. The observed trend is consistent with the magnitude of the 1nn vacancy binding energy. Notably, even at extremely dilute concentrations, such as 10^{-9} of La at 800 K, the vacancy mobility is reduced by ~ 2 orders of magnitude, as shown in Figure 5 (b).

The comparison in Figure 5 (a)-(d) from 600 to 1200 K also shows that the reduced vacancy mobility becomes less significant at higher temperatures and lower concentrations of fission products. Nevertheless, at a high temperature such as 1200 K (Figure 5 (d)), the role of fission products in reducing vacancy mobility remains strong when the concentration of fission products is higher than 10^{-7}. These findings suggest that as fission products infiltrate or diffuse into the matrix of Fe cladding from the fuel under irradiated conditions, the mobility of excess vacancies generated by irradiation is significantly trapped and hindered. This reduced vacancy mobility can lead to an oversaturation of point defects, promoting void nucleation and swelling, thereby exacerbating the degradation induced by FCCI.

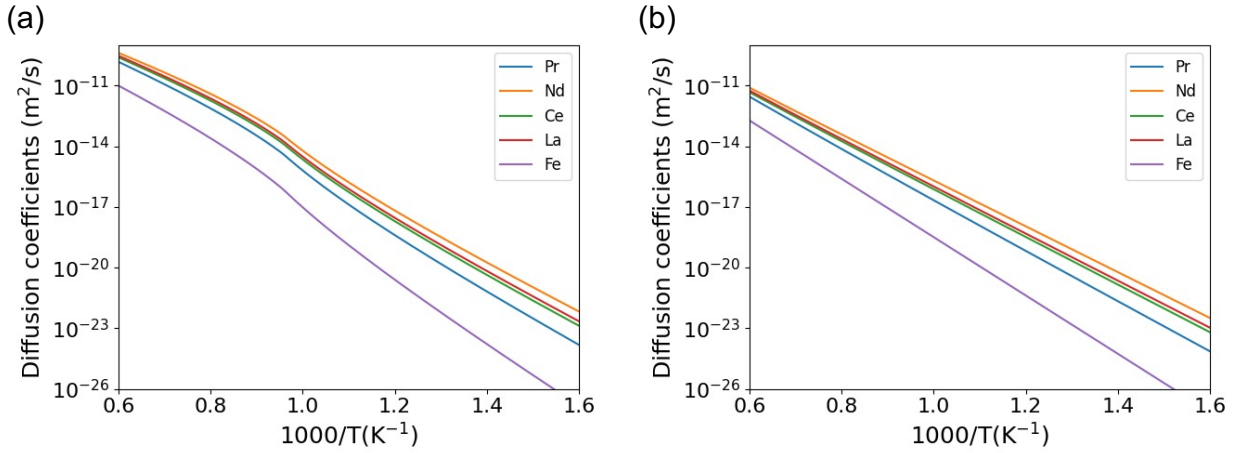

Figure 4. Plots showing the SCMF calculation results of the tracer diffusion coefficients of Pr, Nd, Ce, and La as well as the self diffusion coefficient in (a) bcc Fe with magnetic correction and (b) ferromagnetic bcc Fe.

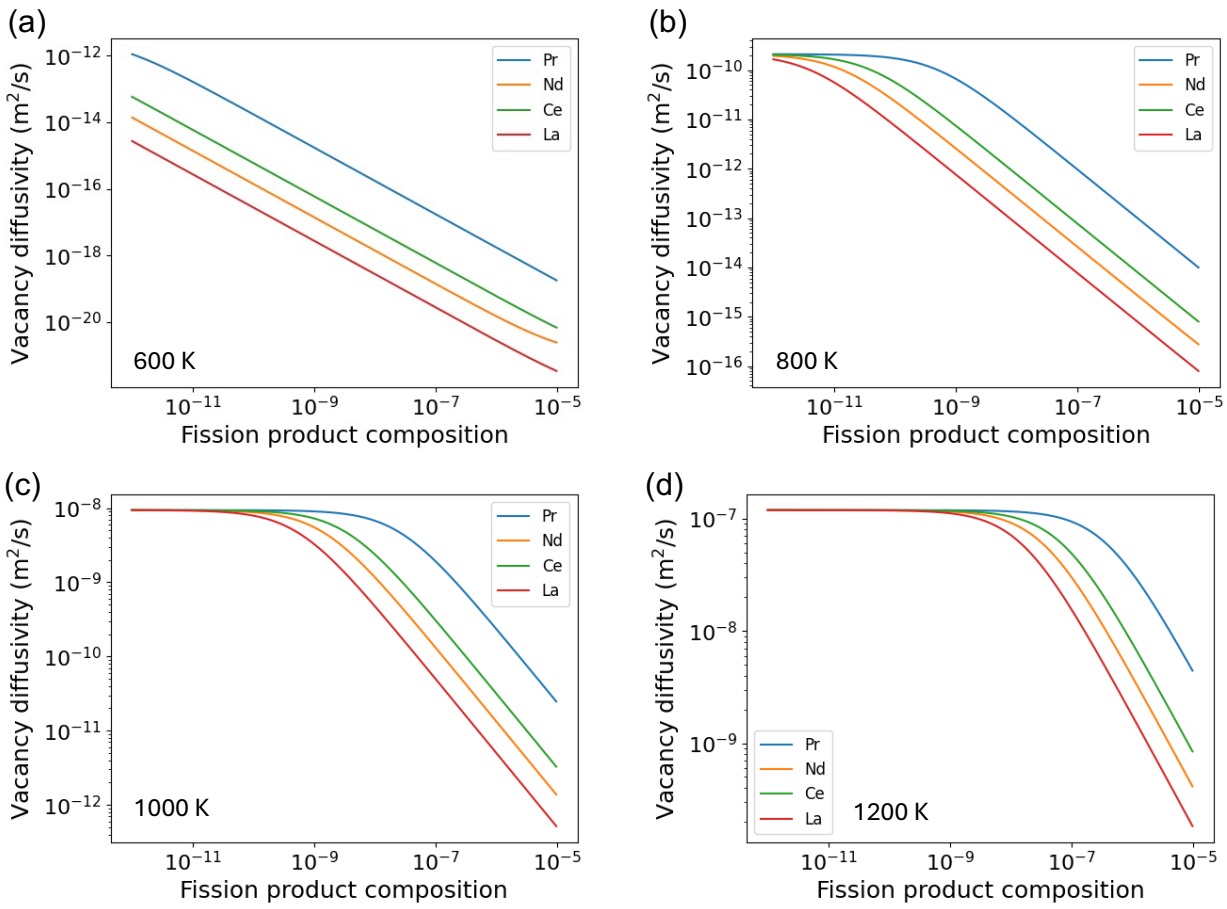

Figure 5. Plots showing the SCMF calculation results of the vacancy diffusivity at (a)600 K, (b)800 K, (c)1000 K, and (d)1200 K as a function of the dilute composition of fission products, Pr, Nd, Ce, and La.

4. Conclusion and future work

The work in this milestone presents a detailed investigation into the diffusion behavior of oversized fission products: Pr, Nd, Ce, and La, within bcc Fe cladding, employing a combination of DFT, NEB method, and SCMF theory. The methodological approach adopted in this work provides an accurate prediction of tracer diffusion coefficients by accounting for long-range interactions and the unique diffusion mechanisms associated with oversized atoms.

Our results reveal significant vacancy binding energies, particularly with the 1st and 2nd nearest neighbors, which diminish beyond the 5th nearest neighbor for all fission products. La exhibits the strongest binding affinity, followed by Nd, Ce, and Pr. The CI-NEB calculations indicate significant high barriers for the dissociation of 1nn vacancy-solute pairs for all fission products, which correlate to the strong binding or trapping effect observed.

The tracer diffusion coefficients of these fission products were derived in Arrhenius form, providing valuable insights into their rate processes and the kinetics of fission product infiltration into the cladding matrix. The activation energies for tracer diffusion in ferromagnetic bcc Fe for Nd, La, Ce, and Pr are 2.25, 2.31, 2.34, and 2.47 eV, respectively. The calculated tracer diffusion coefficients indicate that Nd is the fastest diffuser among the investigated fission products, followed by La, Ce, and Pr. Despite variations in diffusivity, the overall diffusion behaviors of these fission products exhibit similarities due to their oversized nature and comparable binding interactions with vacancies. Note that the significant trapping effect of vacancies by fission products indicates the potential for reduced vacancy mobility, leading to an oversaturation of point defects, void nucleation, and swelling. These effects are critical issues for cladding materials subjected to irradiation. The strength of trapping follows the order of La, Nd, Ce, and Pr, consistent with the trend in the magnitude of 1nn vacancy binding energy.

The insights gained from this study are important for understanding the long-term performance and safety of Fe-based cladding materials in nuclear reactors. The advanced computational methods provide a robust framework for accurately modeling the diffusion behavior of oversized atoms. Future work will includes the computation modeling of fission product transport for bcc Mo. Additionally, exploring the diffusion behavior of other fission products, alloys (e.g., Fe-Mo), and potential synergistic effects of fission products will be essential for comprehensive assessments for advanced development of cladding materials. The development of new cladding materials with enhanced resistance to fission product infiltration and reduced susceptibility to FCCI will be critical in advancing nuclear reactor technology and ensuring long-term operational safety.

Bibliography

[1] Dennis D Keiser Jr. “Fuel cladding chemical interaction in metallic sodium fast reactor fuels: A historical perspective”. In: *Journal of Nuclear Materials* 514 (2019), pp. 393–398.

[2] Robert D Mariani et al. “Lanthanides in metallic nuclear fuels: Their behavior and methods for their control”. In: *Journal of Nuclear Materials* 419.1-3 (2011), pp. 263–271.

[3] Christopher Matthews et al. “Fuel-cladding chemical interaction in U-Pu-Zr metallic fuels: a critical review”. In: *Nuclear Technology* 198.3 (2017), pp. 231–259.

[4] Dennis D Keiser. “3.15-metal fuel-cladding interaction”. In: *Comprehensive Nuclear Materials: Volume 1-5*. Elsevier, 2012, pp. 423–441.

[5] Yeon Soo Kim, GL Hofman, and AM Yacout. “Migration of minor actinides and lanthanides in fast reactor metallic fuel”. In: *Journal of Nuclear Materials* 392.2 (2009), pp. 164–170.

[6] Alan R Allnatt and Alan B Lidiard. *Atomic transport in solids*. Cambridge University Press, 2003.

[7] Jean-Louis Bocquet, Caroline Barouh, and Chu-Chun Fu. “Migration mechanism for oversized solutes in cubic lattices: The case of yttrium in iron”. In: *Physical Review B* 95.21 (2017), p. 214108.

[8] Thomas Schuler, Luca Messina, and Maylise Nastar. “KineCluE: A kinetic cluster expansion code to compute transport coefficients beyond the dilute limit”. In: *Computational Materials Science* 172 (2020), p. 109191.

[9] Maylise Nastar. “A mean field theory for diffusion in a dilute multi-component alloy: a new model for the effect of solutes on self-diffusion”. In: *Philosophical magazine* 85.32 (2005), pp. 3767–3794.

[10] A.D. Le Claire. “Solute diffusion in dilute alloys”. In: *Journal of Nuclear Materials* 69-70 (1978), pp. 70–96. ISSN: 0022-3115. DOI: https://doi.org/10.1016/0022-3115(78)90237-4. URL: https://www.sciencedirect.com/science/article/pii/0022311578902374.

[11] Luca Messina et al. “Exact ab initio transport coefficients in bcc Fe-X (X= Cr, Cu, Mn, Ni, P, Si) dilute alloys”. In: *Physical Review B* 90.10 (2014), p. 104203.

[12] Luca Messina et al. “Solute diffusion by self-interstitial defects and radiation-induced segregation in ferritic Fe–X (X= Cr, Cu, Mn, Ni, P, Si) dilute alloys”. In: *Acta Materialia* 191 (2020), pp. 166–185.

[13] Jia-Hong Ke and Benjamin W Spencer. “Cluster dynamics modeling of Mn-Ni-Si precipitates coupled with radiation-induced segregation in low-Cu reactor pressure vessel steels”. In: *Journal of Nuclear Materials* 569 (2022), p. 153910.

[14] Jia-Hong Ke. “Microstructure modeling of nuclear structural materials: Recent progress and future directions”. In: *Computational Materials Science* 230 (2023), p. 112503.

[15] G. Kresse and J. Hafner. “Ab initio molecular dynamics for liquid metals”. In: *Phys. Rev. B* 47 (1 1993), pp. 558–561. DOI: 10.1103/PhysRevB.47.558. URL: https://link.aps.org/doi/10.1103/PhysRevB.47.558.

[16] G. Kresse and J. Furthmüller. “Efficient iterative schemes for ab initio total-energy calculations using a plane-wave basis set”. In: *Phys. Rev. B* 54 (16 1996), pp. 11169–11186. DOI: 10.1103/PhysRevB.54.11169. URL: https://link.aps.org/doi/10.1103/PhysRevB.54.11169.

[17] Jia-Hong Ke, George A. Young, and Julie D. Tucker. “Ab initio study of phosphorus effect on vacancy-mediated process in nickel alloys – An insight into Ni2Cr ordering”. In: *Acta Materialia* 172 (2019), pp. 30–43. ISSN: 1359-6454. DOI: https://doi.org/10.1016/j.actamat.2019.04.036. URL: https://www.sciencedirect.com/science/article/pii/S1359645419302381.

[18] Jia-Hong Ke and Julie D. Tucker. “First-principles study of 3sp impurity (S, P, Si, Al) effects on vacancy-mediated diffusion in Ni and Ni-33Cr alloys”. In: *Computational Materials Science* 214 (2022), p. 111768. ISSN: 0927-0256. DOI: https://doi.org/10.1016/j.commatsci.2022.111768. URL: https://www.sciencedirect.com/science/article/pii/S0927025622004815.

[19] J.D. Tucker et al. “Ab initio-based diffusion theory and tracer diffusion in Ni–Cr and Ni–Fe alloys”. In: *Journal of Nuclear Materials* 405.3 (2010), pp. 216–234. ISSN: 0022-3115. DOI: https://doi.org/10.1016/j.jnucmat.2010.08.003. URL: https://www.sciencedirect.com/science/article/pii/S0022311510003715.

[20] P. E. Blöchl. “Projector augmented-wave method”. In: *Phys. Rev. B* 50 (24 1994), pp. 17953–17979. DOI: 10.1103/PhysRevB.50.17953. URL: https://link.aps.org/doi/10.1103/PhysRevB.50.17953.

[21] G. Kresse and D. Joubert. “From ultrasoft pseudopotentials to the projector augmented-wave method”. In: *Phys. Rev. B* 59 (3 1999), pp. 1758–1775. DOI: 10.1103/PhysRevB.59.1758. URL: https://link.aps.org/doi/10.1103/PhysRevB.59.1758.

[22] John P. Perdew, Kieron Burke, and Matthias Ernzerhof. “Generalized Gradient Approximation Made Simple”. In: *Phys. Rev. Lett.* 77 (18 1996), pp. 3865–3868. DOI: 10.1103/PhysRevLett.77.3865. URL: https://link.aps.org/doi/10.1103/PhysRevLett.77.3865.

[23] Graeme Henkelman and Hannes Jónsson. “Improved tangent estimate in the nudged elastic band method for finding minimum energy paths and saddle points”. In: *The Journal of Chemical Physics* 113.22 (Dec. 2000), pp. 9978–9985.

[24] Graeme Henkelman, Blas P. Uberuaga, and Hannes Jónsson. “A climbing image nudged elastic band method for finding saddle points and minimum energy paths”. In: *The Journal of Chemical Physics* 113.22 (Dec. 2000), pp. 9901–9904. ISSN: 0021-9606.

[25] Mats Hillert and Magnus Jarl. “A model for alloying in ferromagnetic metals”. In: *Calphad* 2.3 (1978), pp. 227–238.